

Theoretical and Experimental approach to Rolling Contact Fatigue in high-speed railways.

J. Kuszczak, L. Reis, B. Li and M. Freitas

Instituto Superior Técnico, ICEMS & Dept. of Mechanical Engineering, Technical University of Lisbon; Av. Rovisco Pais, 1049-001 Lisboa, Portugal; E-mail: luis.g.reis@ist.utl.pt; mfreitas@dem.ist.utl.pt

***ABSTRACT.** Railway sector places an important role in the means of transportation and Rolling Contact Fatigue (RCF) is a growing problem in many situations. Present review focuses on analytical, numerical and experimental approach to the problem. Hertz Theory was applied firstly to calculate the curvature of ellipse of contact and the stresses governing rolling contact between wheel and rail. Following, the numerical FE analysis were implemented with the respective loads, boundary conditions and material properties. Finally, multiaxial fatigue tests were carried out and the results were compared to few critical plane models. The contact zone was studied for semi-elliptical shape, governed with multiaxial, out- of- phase state of stress with constant change in directions of principal stresses occurring due to rolling.*

INTRODUCTION

Railways still play a key role as a public transport facility, as well as a mean for transport of goods. The need for faster relocation and capacity of trains, Rolling Contact Fatigue (RCF) becomes a growing problem, which costs EU some hundred million Euros annually [1, 2]. Cyclical passage of the wheels over the rails causes significant wear over both elements, which in time may result in fatigue cracks. If the fissures were not detected in its early stages, they might lead to the failure of the components. Initially the cracks appear as small head checks which later take the shape of a V, U, W, Y, or X when looking at the top of the rail surface. Distortions develop through the microstructure of the rail head, mainly due to forces generated by the conicity of the wheel profile, friction and lubrication effects and also due to the inclination of the track installation [3, 4, 5].

The purpose of this research is to study steady state, single, rolling contact conditions between rail and wheel and how they affect the wear and cracking processes of the affected components. The recurring theme is of prime importance for developing a holistic understanding of how rail and wheel interact in the contact.

This paper makes a full approach to the subject, starting with an analytical approach based on Hertz Theory, followed by a numerical Finite Element assessment, to compare

with the experimental results of multiaxial tests presented at the end. The data obtained in experimental tests are also correlated to several critical plane models.

ANALYTICAL APPROACH

- Stress analysis under rolling contact condition

During a single revolution of the wheel, elements are subjected to a cycle of stress. The values range from zero (for the points outside the contact zone), to maximum state of stress (for center point of the contact area). This effect causes a semi-elliptical contact pressure distribution [2], as is shown in the sequence of Figure 1, one wheel rolling from left side to right side. At the Time 1, the material element A under the wheel is only subjected to compressive stress without shear stress, but the neighbor element B is subjected to shear stress, and element C is also subjected to shear stress, but a very small value because it is far away from the contact point. When the wheel run to the next position, Time 2, the element B is subjected to only compressive stress, but the neighbor elements A and C are subjected to shear stress. When the wheel run to the position Time 3, the element C is subjected to only compressive stress, but the neighbor element B is subjected to shear stress, element A is also subjected to a very small shear stress, because it is far away from the contact point. Therefore, one material element (for example element A) is subjected to the maximum compressive stress at Time 1 and the maximum shear stress at Time 2, which are non-proportional normal and shear stresses as shown in Figure 2. The value of the maximum shear stress is about 25% of the maximum compressive stress. Similar to the above discussions about the stress distributions in the rail, the stress distributions in the sub-surface of the wheel are also subjected to non-proportional stresses as shown in the Figure 2, but there are differences of the maximum stress values between the wheel and rail, due to the effect of the radius R (R is considered as infinite for the rail).

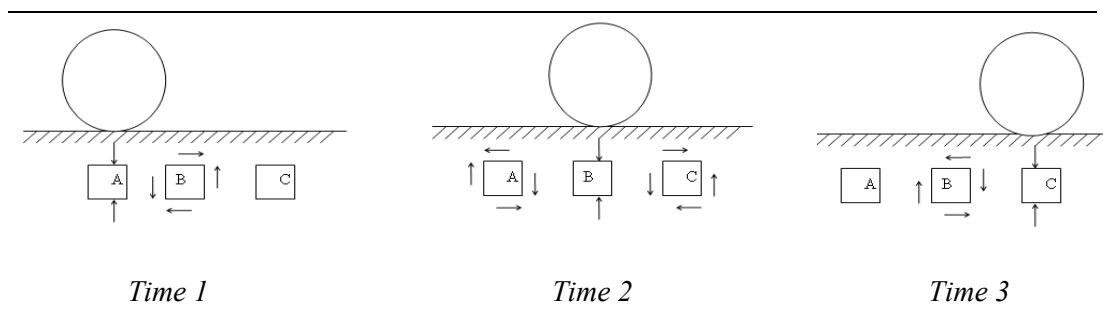


Figure 1. Stresses caused by rolling contact.

Theoretical basis for steady state wheel-rail rolling contact conditions are contained within assumptions of Hertzian Contact Theory, named after German scientist Heinrich Hertz, who developed it in 1882 [6]. Theory of elastic deformation is used to calculate contact geometry and contact stresses, relating the circular/ elliptical contact area of two spheres, or between sphere and a plane to the elastic deformation properties of the

materials [7]. The calculation was mainly based on [8] and [9], but minding other important reviews strictly concerning rail/wheel contact problem [10, 11].

Rail and wheel are held in contact by a force $F= 84268\text{N}$. This value is a half of a maximum load supported by a shaft of an AVE S-101 carriage. After applying a force, the point of contact expands to an ellipse with half- axes a and b , calculated as follows:

$$a, b = K_{a,b} \sqrt[3]{F} \quad (1)$$

where:

$$K_{a,b} = \left[\frac{3}{8} \frac{(1-\nu_1^2)/E_1 + (1-\nu_2^2)/E_2}{(1/R_1) + (1/R_2)} \right]^{1/3} \quad (2)$$

Symbols $\nu_1= 0,3$ and $\nu_2= 0,3$ are Poisson's ratios for wheel and rail respectively. $E_1= 210$ [GPa] and $E_2= 210$ [GPa] are elastic moduli of the bodies. Three- dimensional model was divided in two separate 2D cases in order to facilitate computation of the contact area, see Fig. 2. Dimensions of semi- axis of the ellipse are presented in Table 1, together with radii of curvature R_1 and R_2 of the bodies.

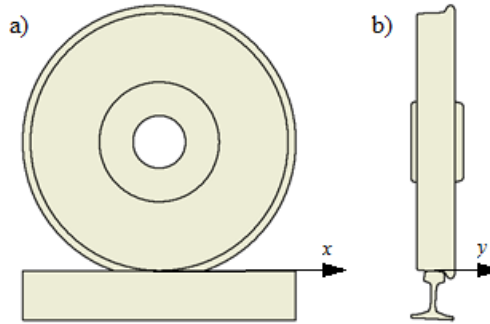


Figure 2. Two- dimensional models: a) Side view, b) Front view

Table 1. Geometry parameters used for the calculation and values of half-axes

	Wheel Radius R_1 [m]	Rail Radius R_2 [m]	Half-axes [mm]
Side View Contact	0,46	∞	a= 5,01
Front View Contact	∞	0,3	b= 4,35

The maximum contact pressure p_{max} acts at the center of the elliptical contact area and is computed in eq. (3). Principal Stresses and Maximum Shear Stress are computed as present in eq(s) (4) to (7), and considering in the critical section $\zeta_b= z/b \approx 0,50$.

$$p_{max} = \frac{3F}{2\pi ab} \quad (3)$$

$$\sigma_x = \sigma_1 = -2v_1 p_{max} \left[\sqrt{1 + \zeta_b^2} - |\zeta_b| \right] \quad (4)$$

$$\sigma_y = \sigma_2 = -p_{max} \left[\left(\frac{1+2\zeta_b^2}{\sqrt{1+\zeta_b^2}} \right) - 2|\zeta_b| \right] \quad (5)$$

$$\sigma_z = \sigma_3 = -p_{max} \frac{1}{\sqrt{1+\zeta_b^2}} \quad (6)$$

$$\tau_{max} = \frac{\sigma_x - \sigma_z}{2} \quad (7)$$

NUMERICAL APPROACH

The main purpose for this section was preparing a static simulation of contact between monoblock wheel with stabilized profile and the rail UIC60 to compare with analytical and experimental results. Both elements were designed with the aid of Autodesk Inventor 2013 and exported without any compatibility problems to Autodesk Simulation Multiphysics 2013 in order to run Finite Element Analysis of contact.

The size of investigated bodies was reduced to most affected areas. This action helps to increase computational force of the computer, which saves time of simulation and protects from software errors. Bibliography investigation indicated that brick type element (ABAQUS type: C3D20) is most adequate for this simulation [7, 12]. Automatic mesh size was applied, followed by mesh refinement of 0,5mm for the most critical parts of the profiles, as made by other authors [13, 14]. Mesh results, as well as applied loads and boundary conditions are presented on Fig. 3. Structural static stress analysis with linear material models confirmed elliptical shape of the contact. Distribution of normal stress is presented on Fig. 3.

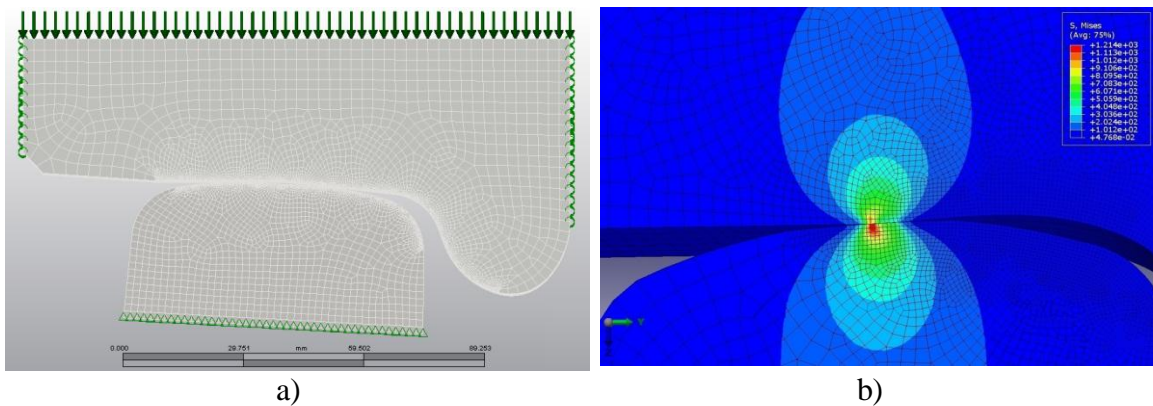


Figure 3. a) Mesh and loading conditions; b) Normal stress distribution under RCF.

EXPERIMENTAL APPROACH

Methodology

The toroidal samples used for experiments were provided by Alstom Spain. Chemical constitution of the steel is presented in the Table 2. As most of the steels used for rail/wheels production, the material was classified as non-alloy pearlitic steel with medium carbon content [15]. The geometry of toroidal specimen is presented on Fig. 4.

Table 2. Chemical composition of selected steel

Chemical Composition [%]										
Fe	C	Si	Cu	Al	Pb	Sn	V	Zn	Zr	Ti
97,8	0,49	0,25	0,12	0,03	<0,03	<0,01	<0,005	<0,003	<0,002	<0,001
Mn	Cr	Ni	Mo	P	W	As	S	Ca	Sb	B
0,74	0,26	0,18	0,06	0,01	<0,01	<0,01	<0,005	<0,003	<0,002	<0,001

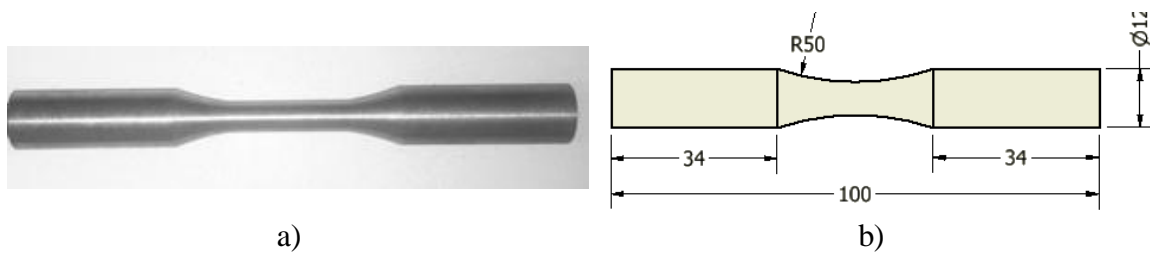


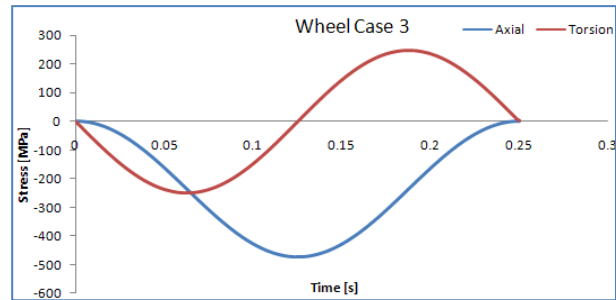
Figure 4. Geometry of toroidal sample [mm]

Biaxial, servo-hydraulic testing machine type 8874 produced by INSTRON was used to perform experimental tests. Personal Computer equipped with Windows 2000 operating system and software 32-bit INSTROM MAX ver. 7.0 served for saving the data from the machine, see Fig. 5. All the tests were carried out in ambient temperature and 50% humidity. Three different types of loading were applied for investigation purpose, see Fig.(s) 5 and 6. Case I is a proportional loading, while Case II is non- proportional 90° out of phase loading. Both these Cases serve as a reference to Wheel-Rail Case, which simulates the loads occurring when the wheel is interacting with the rail.

Fractographic investigation was performed on OPTICA microscope, model SZM-2, and an analog eyepiece- video camera (Reference: 571205) produced by Jeulin. The magnitude used was up to 45x (Eyepiece: 10x, Object lens: 4,5x).

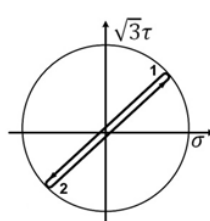


a)

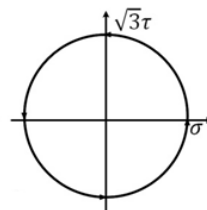


b)

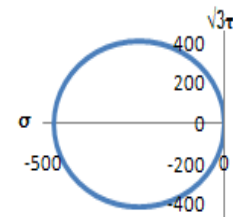
Figure 5. a) Biaxial Fatigue Testing System; b) Non-proportional loading caused by RC.



Case I



Case II



WheelCase 3

Figure 6. Multi-axial loading paths applied.

RESULTS

The results of multi-axial fatigue tests are presented in Table 3. Non-proportional types of loading create noticeably higher axial and shear stresses than proportional in-phase loading. Wherein, Case II arises as the most destructive case for selected steel. The specimens under this loading path have significantly shorter fatigue life than other samples, for the same equivalent von Mises stress. Samples from Wheel-Rail loading case tend to survive significantly more cycles of all.

Table 3. Results of Multi-axial Fatigue Tests carried out.

Loading Case	Specimen Identification	Axial Stress [MPa]	Shear Stress [MPa]	Fatigue Life N_f
Case I	D1	289,5	167,1	139450
Case II	F1	434,3	250,7	11800
	B1	372,4	215,0	51878
Wheel-Rail Case	A1	524,2	277,5	111000
	E1	473,9	250,7	442000
	C1	384,9	208,9	1150000

Final part of the experimental procedure was devoted to determination of critical planes for selected loading type. The assessment of the fractured surface is an essential tool to identify the root cause of the failure. Fig. 7a) illustrates a fractured surface of a specimen subjected to a Wheel-Rail Case loading under fatigue tests and Fig. 7b) shows the measured angle due to the crack concerning this loading path.

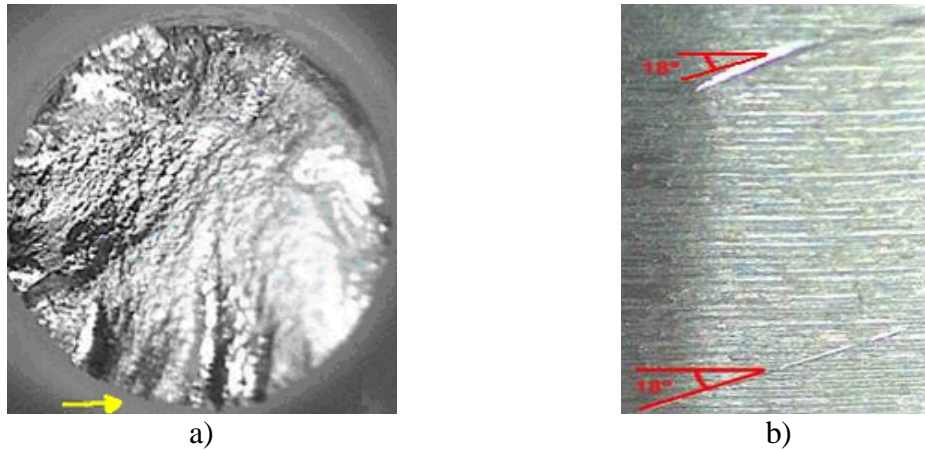


Figure 7 – Wheel-Rail Case fractured surface: a) crack origin; b) measured angle.

From figure 7, it is possible to identify the typical fatigue fracture areas (crack initiation zone, crack propagation and final rupture zone) and roughness. The measured angle in this loading case was -18° . The measured angles from all loading path are compared to few theoretical models predicting crack initiation plane angle, where damage parameter reaches maximum value, see Table 4, [16].

Table 4. Comparison of the critical plane angles

	Case I	Case II	Wheel-Rail Case
Measured	-15	0	-18/ -20
Findley	-12/ 61	0	-81/ 81
Fatemi- Socie	-9/ 59	0	-78/ 78
Brown- Miller	-15/ 64	0	-84/ 84
SWT	25	0	-48/ 48

As can be seen from Table 4, only in Case II loading, measured critical plane angle corresponds fully with results computed from the theoretical models. However, angle values for Case I are similar to each other and are considered valid, except for the tensile based SWT model. Wheel-Rail Case loading type is an exception, measured angle do not match with calculated ones, and sometimes more than one crack occurs keeping the same slope, as shown in figure 7b).

CONCLUSIONS

- Normal and shear stress distributions in the sub-surface under rolling contact condition are analyzed both theoretically and numerically, main and secondary stresses are identified and the non-proportional stress state is also characterized;
- Experimental fatigue tests were carried out under the real non-proportional stress state, both fatigue lives and early crack growth angles were analyzed and measured;
- Critical plane models allow to predict critical plane orientations; results obtained for loading cases I and II agree with the predicted ones. Values obtained for loading Wheel-Rail case do not match with predicted ones.

Further research work is ongoing to improve the models for the predominantly compressive stress states such as those of RCF.

ACKNOWLEDGMENTS

The authors of this paper are grateful to FCT - Fundação para Ciência e Tecnologia (Portuguese Foundation for Science and Technology), for financial support through the project PTDC/EME-PME/100204/2008.

REFERENCES

1. Cannon, D.F., Pradier, H. (1996) *Wear*, **191**, 1-13.
2. Reis, L., Santos, P., Li, B., Freitas, M. (2012) *Proc. 1st Int. Conf. Int. J. Structural Integrity*, Paper 24, 137-142, Rodopoulos, C. (Ed.), Monash University, Australia.
3. Ringsberg, J.W., Loo-Morrey, M., Josefson, B.L., Kapoor, A., Beynon, J.H. (2000) *Int. J. of Fatigue*, **22**, 205-215.
4. Peixoto, D.F.C., Castro, P.M.S.T., Ferreira, L.A.A. (2012) In: *Proceedings of the 1st International Conference on Railway Technology: Research, Development and Maintenance*, Paper 87, Pombo, J. (Ed.), Civil-Comp Press, Stirlingshire, Scotland
5. Steenbergen, M.J.M.M. (2012) In: *Proceedings of the 1st International Conference on Railway Technology: Research, Development and Maintenance*, Paper 96, Pombo, J. (Ed.), Civil-Comp Press, Stirlingshire, Scotland
6. Barbera, J.R., Ciavarell, M. (2000) *Int. J. of Solid and Structures*, **37**, 29-43.
7. Peixoto D. (2008) MSc Thesis, Faculty of Engineering, University of Porto, Portugal.
8. Budynas, R.G., Nisbett, J.K. (2006) *Shigley's Mechanical Engineering Design*, 8 Edition, McGraw-Hill Primis (Ed.)
9. Johnson, K. L. (1987) *Contact Mechanics*, Cambridge University Press (Ed.),
10. Wiest, M., Kassac, E., Davesa, W., Nielsenc, J.C.O., Ossberger H. (2008), *Wear*, **265**, 1439-1445.
11. Zerbst, U., Lundén, R., Edel, K.O., Smith, R.A. (2009) *EFMech.*, **76**, 2563-2601.
12. Santos, P. (2011), MSc. Thesis, Technical University of Lisbon, IST, Portugal.
13. Sladkowski, A., Sitarz, M. (2005) *Wear*, **258**, 1217-1223.
14. Jianxi, W., Yude, X., Songliang, L., Liying, W. (2011) *IJ. of Fatigue*, **33**, 212- 216.
15. Pointer, P. (2008) *Wear*, **265**, 1373-1379.
16. Li, B., Reis, L., Freitas, M. (2006) *Int. J. of Fatigue*, **28**, 451- 457.